Observing system simulation experiments exploring potential spaceborne deployment options for a differential absorption radar measuring marine surface pressures

N.C. Privé[1,2], Matthew McLinden[2], Bing Lin[3], G. M. Heymsfield[2], Xia Cai[3], Steven Harrah[3]

[1]Goddard Earth Sciences Technology and Research II, Morgan State University, Baltimore MD
[2]Goddard Space Flight Center, National Aeronautics and Space Administration, Greenbelt MD
[3]Langley Research Center, National Aeronautics and Space Administration, Hampton, VA

Key Points:

- The greatest observation impacts are found in the southern hemisphere extratropics, with neutral impacts in the tropics.
- The most beneficial observation impacts occur with a four-satellite platform of non-scanning instruments.
- Beneficial impacts are found for a wide range of observation error magnitudes.

Corresponding author: Nikki Privé, nprive@alum.mit.edu

Abstract

A new technology for remote measurements of marine surface pressure has been proposed, employing a V-band differential absorption radar and a radiometric temperature sounder to calculate the total column atmospheric mass. Observing System Simulation Experiments (OSSEs) are performed to evaluate the potential impact of Spaceborne Marine Surface Pressure (SMSP) on Numerical Weather Prediction (NWP). These experiments build on prior efforts (Privé, McLinden, et al., 2023), but with an updated version of the OSSE framework and with more sophisticated simulation of the SMSP observations and a longer experiment period. Several different instrument configurations are compared, including both scanning and non-scanning orbits. SMSP impacts are calculated for analysis quality and forecast skill, and a forecast sensitivity observation impact tool is employed to place SMSP observations in context with the global observing network. The effects of rain contamination on observation quality are explored. Different magnitudes of simulated SMSP observation error are tested in the context of data assimilation to show the range of potential behaviors. Overall, SMSP observations are found to be most beneficial in the southern hemisphere extratropics, with statistically significant forecast improvements for the first 72 hours of the forecast. A constellation of four non-scanning SMSP satellites is found to outperform a single scanning instrument with a 250 km wide swath.

Plain Language Summary

Measurements of surface pressure are very useful for weather prediction because they tell us about phenomena such as winter storms, as well as large scale atmospheric circulation patterns. Over the ocean, the only surface pressure measurements currently come from buoys and some ships, but these measurements are very far apart. Recently, some new radar technology is under development that would allow ocean surface pressures to be remotely retrieved from aircraft or satellites. In this work, these proposed new radar surface pressure measurements are simulated and tested in a weather forecast model. Several different configurations of an orbiting spaceborne radar are simulated and compared to find out how much the radar data would improve weather forecasts. The results show that a constellation of four smaller radar satellites has the most improvement on weather prediction. The effect of instrument noise was also tested, and it was found that the radar was helpful for weather forecasts for a wide range of instrument performance.

1 Introduction

It can be challenging to determine instrument design requirements for the development of novel platforms that observe the atmosphere and oceans. When no similar instrument types exist, there can be significant unknowns as to the optimal sampling strategies or necessary accuracy levels of the new instrument. Observing System Simulation Experiments (OSSEs) can be used to test different instrument configurations in a realistic setting to characterize the impacts of new instrument designs on Numerical Weather Prediction (NWP).

OSSEs are modeling experiments in which all aspects of the global observing network are simulated. The real atmosphere-ocean system is replaced with a simulated version, called a Nature Run. Every instrument type currently used in NWP is simulated to generate 'synthetic' observations intended to replicate the global observing system in the world of the Nature Run. These synthetic observations include added simulated observation errors to replicate the error characteristics of real observations. New instrument types are then simulated and tested within the emulated world of the OSSE, where characteristics of the new data can be directly manipulated and evaluated.

Up until now, marine surface pressure measurements have only been possible from in situ instruments such as ships, buoys, and ocean platforms. However the spatial distribution of these instruments is far from uniform, with most observations located near coastlines, and far fewer observations available in the open ocean. Many drifting buoys do not report surface pressures (Centurion et al., 2017), and ship-based pressure observations can be subject to large errors depending on the type of vessel and the reporting method (Ingleby, 2010).

Despite the dearth of in situ marine surface pressure observations, previous studies have indicated that this dataset is important for NWP. A data denial experiment in which all marine surface observations were omitted from the European Centre for Medium-range Weather Forecasts (ECMWF) operational system found a significant decrease in forecast skill in the Southern Hemisphere (Radnóti et al., 2012). Horányi et al. (2017) removed only drifting buoy data from the ECMWF operational system and found that the root-mean-square surface pressure errors increased by as much as 30% regionally. Forecast skill declined globally for up to 2-3 forecast days when the drifting buoys were omitted. Surface pressure observations from drifting buoys were the subject of data denial experiments by Ingleby and Isaksen (2018), and these observations were found to improve NWP forecasts, particularly in extratropical regions of cyclogensis. Reynolds et al. (2023) examined the impacts of buoy surface pressures as part of the Atmospheric River Reconnaissance Program, and found that drifting buoys in the north Pacific have the greatest impacts in regions of tight pressure gradients associated with substantial water vapor transport, such as fronts and atmospheric rivers.

Some existing technologies have been investigated for remote sensing of surface pressure observations, but a satisfactory option has not been found. Scatterometer winds have been suggested as a possible method of determining surface pressures using hydrostatic balance with surface winds, but this technique can only be used to calculate pressure gradients rather than total pressures, and is only possible over a limited range of wind speeds. Healy (2013) showed that Global Navigation Satellite System Radio Occultation (GNSS-RO) observations can be employed to constrain the surface pressure field and improve forecast skill to a certain degree in the absence of in-situ surface pressure observations. However, Healy illustrated the sensitivity of remotely sensed surface pressure data to biases from the NWP model and from other data types that can compromise the use of these data types.

A novel instrument for remote sensing of marine surface pressures is expected to undergo airborne engineering test flights in 2024, funded by the National Aeronautics and Space Administration (NASA) Earth Science Technology Office (ESTO). The Microwave Barometric Radar and Sounder (MBARS) instrument is currently under development by the NASA Goddard Space Flight Center, NASA Langley Research Center, and Tomorrow.io under the Instrument Incubator Program. This instrument uses combined active and passive microwave sensors operating at the O_2 absorption V band (64–70 GHz) to measure atmospheric column O_2 amounts in no- or light-rain conditions using a differential absorption method (Lin and Hu (2005); Lawrence et al. (2011); Millán et al. (2014); Lin et al. (2023)). The instrument would measure the O_2 content of the atmosphere, which is proportional to the column dry air mass in a well mixed atmosphere. Along with measurements of atmospheric moisture, the total surface air pressure can be derived. The airborne test flights will include both the V-band differential absorption radar (DAR) and a radiometric temperature sounder. This type of differential absorption radar measurement is used to retrieve surface air pressure primarily in regions without significant precipitation for both airborne and spaceborne measurements.

Spaceborne DAR systems are designed to operate at the 65–70 GHz V-band for atmospheric column O_2 mass measurements. Two DAR frequencies are chosen to be closely-spaced such that atmospheric attenuation other than O_2 and surface reflection are similar but the difference in O_2 absorption is substantial. Thus, when DAR sea surface re-

turns are measured, the effects of the attenuation and reflection are significantly reduced and the differential loss due to atmospheric O_2 is dominant and can be measured by the ratio of frequency-paired DAR signals. However, certain environmental variables such as humidity, clouds, rain, and sea surface conditions could potentially impact the measured power ratio because of the need for very precise sea surface pressure observations (1–2 hPa). Since the absorption and reflectivity of these variables vary nearly linearly with frequency in the closely spaced spectra, a third channel, also with an evenly spaced spectrum at weaker O_2 absorption wavelength, is used to form the second pair for differentiating the differential absorption measurements of the two pairs of channels for the DAR system. This differentiation of differential absorption significantly reduces environmental impacts to a negligible level for sea surface pressure retrievals as shown by Lin et al. (2024).

Privé, McLinden, et al. (2023) performed preliminary OSSE investigations of a spaceborne marine surface pressure (SMSP) instrument, exploring different swath widths of a scanning type orbit. The preliminary studies used a version of the NASA Global Modeling and Assimilation Office (GMAO) NWP OSSE framework based on a version of the NWP model and data assimilation that was quasi-operational in 2018, and simulated observations replicating the global observing network in 2015. Different orbital configurations were tested for an SMSP, and it was shown that remotely sensed surface pressure observations could beneficially impact NWP analyses and forecast skill.

In this study, additional investigations of potential SMSP instruments are carried out in a more recent GMAO OSSE framework. The GMAO OSSE has since been updated to a version of the Goddard Earth Observing System (GEOS) model and Gridpoint Statistical Interpolation (GSI) data assimilation system that were in use in 2022-2023, with simulated observations based on the 2020 global observing network. Notably, this newer quasi-operational NWP system uses a different atmospheric mass for the dry mass constraint that alleviates some issues that were encountered in the preliminary studies. The simulation of the SMSP instrument has been modified to include precipitation contamination and a 50-km footprint for the SMSP instrument.

Several different design characteristics of an SMSP are explored in this manuscript. A single orbit scanning instrument is compared with various configurations of a non-scanning constellation of up to four platforms. The effects of precipitation contamination are evaluated both on a global scale and for case studies of tropical cyclones. Simulated instrument error is tested over a range of error magnitudes and in conjunction with varied observation weighting by the data assimilation system.

The organization of this manuscript is as follows: the GMAO NWP OSSE framework, simulated SMSP observations, and experiment setup are described in Section 2. Results of the experiments are shown in Section 3, and an overall discussion is given in Section 4.

2 Method

2.1 OSSE Framework

The GMAO NWP OSSE framework has been described in detail, validated against real observations, and compared with the previous version of the framework used in prior studies by Privé, McGrath-Spangler, et al. (2023). A brief overview of the OSSE setup is given here.

For the purposes of any OSSE, the real world is replaced with a simulated atmosphere called a Nature Run. The Nature Run is long, free forecast of an atmospheric model and is used both for verification and for generation of simulated observations. In the GMAO OSSE, the GEOS-5 Nature Run (G5NR) was used, having 72 vertical levels, approxi-

mately 7 km horizontal resolution (C1440), and 30 minute temporal output over a two year period. The G5NR employed a model version of GEOS similar to that used for the MERRA-2 reanalysis, and has been extensively validated (Gelaro et al., 2014).

The NWP model used for the experiments was the version of GEOS that was quasi-operational in 2022 and early 2023, run at 25 km horizontal resolution (C360) with 72 vertical levels. Compared to the G5NR, the experiment model version had different resolution, convection and radiation schemes, boundary layer parametrizations, land surface model, and advection and damping schemes. Privé, McGrath-Spangler, et al. (2023) showed that this version of the OSSE has less of a tendency for 'twinning' or insufficient model error compared to the version that was used for the previous SMSP OSSE (Privé, McLinden, et al., 2023). The data assimilation system (DAS) used was the 4-dimensional hybrid ensemble variational (4D hybrid EnVar) GSI.

Simulated observations were generated based on the locations of observations in 2020, but using the G5NR model fields for observed variables, clouds, and rawinsonde drift. A list of simulated data types is given in Table 1. Radiance observations were generated with the Community Radiative Transfer Model (CRTM; Han et al. (2006), Ding et al. (2011)) version 2.2.3 based on the spatiotemporal footprints of real radiance observations. The G5NR cloud fields were used to determine cloud contamination of clearsky radiance types and cloud effects on allsky types (GMI, AMSR2, and MHS). Atmospheric Motion Vectors (AMVs) were located based on the cloud and water vapor fields of the G5NR (R. M. Errico et al., 2020), except for the Himawari platform for which the same locations as real observations were used due to the grid-like distribution of the real Himawari AMVs. GNSS-RO observations were generated using the 2-dimensional Radio Occultation Processing Package (ROPP, Culverwell et al. (2015)). For any observing type that experienced an extended outage in 2020, the 2021 observation locations were substituted during the period of missing data. Details of the methods used to simulate observations are given in R. Errico et al. (2017).

Table 1. Simulated observation types used in the GMAO OSSE framework.

Radiance		Conventional
Instrument	Platform	
AIRS	Aqua	Surface conventional
AMSR2	GCOM W1	Aircraft
AMSU-A	NOAA-15	AMV
AMSU-A	NOAA-18	Rawinsonde
AMSU-A	NOAA-19	Scatterometer
AMSU-A	METOP-A	GNSS-RO
AMSU-A	METOP-B	
AMSU-A	METOP-C	
ATMS	NOAA-20	
ATMS	NPP	
CrIS-FSR	NPP	
CrIS-FSR	NOAA-20	
GMI	GPM	
IASI	METOP-A	
IASI	METOP-B	
MHS	METOP-B	
MHS	METOP-C	
SSMIS	F17	

Simulated observation errors were added to all simulated observing types in order to match the known error characteristics of real observations as best possible (R. Errico et al. (2017), Privé, Errico, and McCarty (2021), Privé, McGrath-Spangler, et al. (2023)). Uncorrelated random error was simulated for all data types, and random correlated errors were selectively applied to certain data types. Vertically correlated errors were applied to sounding observations such as rawinsondes and GNSS-RO as well as AMVs, horizontally correlated errors were applied to clearsky microwave radiance types and AMVs, and channel correlated errors were added to hyperspectral infrared radiances. The magnitude of the simulated errors was calibrated so that the standard deviation of the observation innovations (observation minus background, O-B) was as close to that of real data as possible for each data type. The use of correlated errors on the Control observing network helps to increase the magnitude of the background error and analysis increments, improving the realism of the OSSE framework. Previous work (Privé, Errico, & McCarty, 2021) has shown that the inclusion of simulated correlated observations errors compared to purely uncorrelated errors tends to slightly increase the observation impacts as estimated by Forecast Sensitivity Observation Impact (FSOI, Holdaway et al. (2014)). The increased background error results in more available 'work' for the observations to perform despite the less optimal use of the observations by the data assimilation system due to the inclusion of correlated errors.

An OSSE Control was produced, consisting of three months of analyses and forecasts using only observation types that were ingested in the real world in 2020 for the period of July-September of the second year of the G5NR. The performance of this system has been validated and described in Privé, McGrath-Spangler, et al. (2023). Figure 1 compares the OSSE and real data FSOI using a 24-hour forecast total wet energy error norm for three different regions for the months of July and September (August is omitted due to real data outages of several platforms during 2020), where negative impacts indicate a reduction in 24-hour forecast error. Total wet energy is defined as the sum of the kinetic energy, thermal energy, potential energy, and latent heat energy. Three regions are considered for calculating forecast impacts and FSOI: Northern Hemisphere Extratropics (20°N-90°N, NHEX), Southern Hemisphere Extratropics (20°S-90°S, SHEX), and the Tropics (20°S-20°N).

In general, observation impacts in the OSSE are somewhat smaller in magnitude than for real observations due to weaker model error growth in the OSSE framework, but the relative ranking of different data types is well-preserved in the OSSE. Notable differences between the OSSE and real include anomalously weak impacts from rawinsondes (RAOB), ATMS, and AMSU-A. However AMVs tend to have greater impact in the OSSE compared to Real. These findings are described in greater detail in Privé, McGrath-Spangler, et al. (2023).

2.2 Simulated SMSP Observations

SMSP observations were simulated using the G5NR surface pressure field at prescribed orbital locations. In contrast to the preliminary studies described in Privé, McLinden, et al. (2023), a 50 km diameter observation footprint was implemented along with screening for heavy precipitation. The 50 km footprint is based on the anticipated spatial averaging of a spaceborne sensor required to achieve high-precision atmospheric pressure retrievals. The footprint was calculated using the areal-weighted mean surface pressure over all G5NR gridpoints that fall within 25 km distance from the center point. The total land area within the footprint was calculated, and if more than 5% of the footprint contained landmass, then the observation was omitted. Similarly, the observation was omitted if more than 10% of the footprint was covered by sea ice.

While the preferred field of interest for the simulation of rain contamination of the instrument was the maximum instantaneous precipitation within the footprint at the time

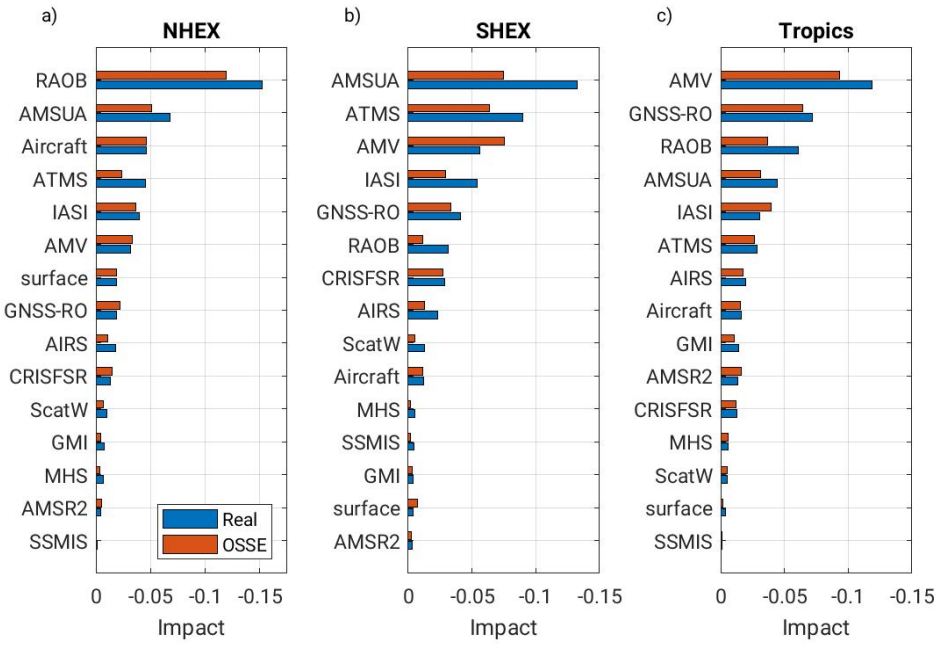


Figure 1. Comparison of FSOI estimates of observation impacts for the OSSE Control compared to real observations from 2020. 0000 UTC forecast cycle impacts on the 24 hour forecast of total wet energy error norm. July and September forecasts are used with August excluded due to real data outages. a) 20N-90N, NHEX; b) 20S-90S, SHEX; c) 20S-20N.

of overpass, this field was not available from the model output. Instead, gridbox net precipitation rates calculated over both cloudy and cloudfree regions were probabilistically converted to instantaneous local rain rates. For each gridpoint within the footprint, the cloud fraction of low clouds was interpolated to the observation time. If at least 5% of the gridpoint was considered to be covered by low clouds, then the local rain rate was calculated by converting the total precipitation in the gridbox to a rainrate that assumes rain only occured in the cloudy areas. A random number λ between 0 and 1 was drawn and used to generate a randomly influenced 'instantaneous rain rate', R_i from the temporally interpolated local rain rate R_t:

$$R_t = R_G/C_F \quad (1)$$

$$R_i = 2\lambda R_t \quad (2)$$

where C_F is the cloud fraction, R_G is the temporally interpolated gridbox net rain rate. If R_i was greater than a chosen threshold value, then that gridpoint was assumed to be contaminated by heavy precipitation, and the entire footprint was omitted. Rain rate, rather than rain water path, is chosen for screening for precipitation contamination as it is a more common metric from satellite radiance observations.

For the purposes of these experiments, this threshold value was set to 1 mm per hour. The use of a 1 mm/hr threshold for rain contamination is fairly restrictive, and offers a lower bound on the expected instrument performance. While the DAR may be able to provide useful information in light rain situations, in moderate to heavy rain conditions, increased atmospheric attenuation might cause a more severe reduction in the signal to noise ratio for the measurement. In these experiments, partial contamination is not considered, and the rain threshold is used solely to determine whether or not a retrieval would be possible.

2.3 Experiment Setup

Several different types of experiments were performed, including evaluation of the effects of precipitation contamination, comparison of different orbital configurations, and characterization of SMSP observation errors. Table 2 details the configurations of all experiments described in this paper. For all SMSP experiments, simulated SMSP data were added to the simulated global observing network and ingested such that the SMSP data were treated similar to buoy or ship surface pressures. This was suitable for these experiments as the SMSP pressures were simulated as if they were retrieved values (Lin et al., 2024). The expectation for real SMSP data is that while the data would initially be assimilated via retrievals, a suitable operator and tangent linear model would be developed to allow direct assimilation of return signals from the DAR.

SMSP assimilation differs from ship and buoy data by the use of greater assigned observation errors for the orbital configuration experiments, with assumed standard deviation of 2 hPa for SMSP compared to 1 hPa which is used quasi-operationally for in situ surface marine observations. While simulated observation errors were added to all other simulated observations, the simulated SMSP data was tested with varying magnitudes of added simulated observation error. The role of assigned observation errors is further explored in section 3.2. The SMSP experiments were compared to the OSSE Control run, which does not include SMSP data, in order to determine the impacts of the SMSP data in the context of the global observing network.

Two different methods of running the DAS were used. For the orbital configuration experiments, the standard method of cycling the DAS was used, where the model is integrated forward in time to produce a new background field that is combined with ingested observational data to produce a new analysis state. This will be referred to as 'full cycling' mode. In this mode, 5-day forecasts are produced once daily starting at 0000 UTC, and FSOI can be generated.

An alternative method of running the DAS, 'standalone' mode, is computationally faster but does not integrate the forecast model between analysis times. Instead, the background field is taken from the OSSE Control and is used to make a new analysis that includes the SMSP data as well as the rest of the global observations. While the background field is not influenced by information from the SMSP observations, this mode can allow many variations of SMSP data to be tested at low expense. Comparison of standalone versus full cycling SMSP impacts shows that the SMSP impacts are approximately 30% weaker overall in the standalone case. Standalone mode was used for testing the precipitation contamination effects and for characterizing the SMSP observation errors. However extended forecasts and FSOI cannot be generated for Standalone cases.

3 Results

Analysis and forecast errors can be calculated by comparing the model fields to the NR fields regridded to the same resolution, as the NR is considered the 'truth' in the OSSE framework. Two metrics are used for calculating the impacts: the Root-Temporal-Mean-Square Error (RTMSE) is used for analysis impacts, where the mean is calculated over four-times-daily cycle times for the experiment period; and Root-Area-Mean-Square Error (RAMSE) is used for forecast impacts, where the area-weighted mean is calculated for each forecast over a specific region. The analysis or forecast error of each experiment run is compared to the OSSE Control analysis or forecast error to determine the change in error resulting from the inclusion of SMSP observations. In order to put SMSP impacts into context, the fractional change in the RAMSE or RTMSE is calculated by normalizing by the Control error as follows

$$RMSE_N = \frac{RMSE_{SMSP} - RMSE_{Control}}{RMSE_{Control}} \tag{3}$$

Table 2. List of experiment configurations. SMSP Error indicates the magnitude of any added simulated observation error for SMSP data. Footprint indicates the simulated size of the instrument footprint. Rain indicates whether rain contamination was applied for the simulated SMSP observations.

Experiment	Scan Type	# Orbits	Cycling	SMSP Error	Footprint	Rain
NOCONT	Scanning	1	Standalone	No	0 km	No
RAINCONT	Scanning	1	Standalone	No	50 km	Yes
SWATH	Scanning	1	Full Cycling	No	50 km	Yes
1-ORBIT	Non-Scanning	1	Full Cycling	No	50 km	Yes
2-ORBIT	Non-Scanning	2	Full Cycling	No	50 km	Yes
4-ORBIT	Non-Scanning	4	Full Cycling	No	50 km	Yes
NOERR	Scanning	1	Standalone	No	50 km	Yes
1-ERR	Scanning	1	Standalone	1 hPa	50 km	Yes
2-ERR	Scanning	1	Standalone	2 hPa	50 km	Yes
4-ERR	Scanning	1	Standalone	4 hPa	50 km	Yes

where $RMSE_N$ is the normalized RAMSE or RTMSE depending on the type of calculation, and subscripts for SMSP or Control indicate the experiment including SMSP observations or the OSSE Control, respectively.

3.1 Precipitation Effects

In order to test the effects of rain contamination on the SMSP data, two comparison datasets were simulated. In the first experiment, 'RAINCONT', the simulated observations were generated with 50 km footprints and rain contamination as described in Section 2.2.2. In the second experiment, 'NOCONT', the simulated observations were generated without accounting for rain contamination, and using only the center point of the footprint to determine the surface pressure observation - this is the method that was used previously in Privé, McLinden, et al. (2023). These two experiments were run in Standalone mode for the month of September, using background fields taken from the Control run. This time period was selected in order to compare the impacts of the SMSP instrument on tropical cyclones with and without rain contamination. Due to the use of Standalone mode, the analysis fields for any cycle time can be directly compared to isolate the effects of the SMSP data because the same background fields are used for both the experiments and the Control. The orbit selected was based on a single scanning instrument type configuration with 250 km wide swath, as illustrated in Figure 2a, which uses the ATMS orbit as a model with scan angles and along-track spacing selected to achieve approximately 50 km spacing between observations. Simulated SMSP errors were not added to the SMSP observations in these experiments.

3.1.1 Rain Contamination

Comparing the results of the NOCONT and RAINCONT experiments shows that including the effects of rain contamination on SMSP observations reduces the number of observations passing quality control by approximately 4-5% (not shown). In the extratropics, the majority of rain-contaminated observations are generally clustered near synoptic features such as frontal rainbands. In the tropics, some clustering is noted near large-scale features such as the Inter-Tropical Convergence Zone (ITCZ), but there are

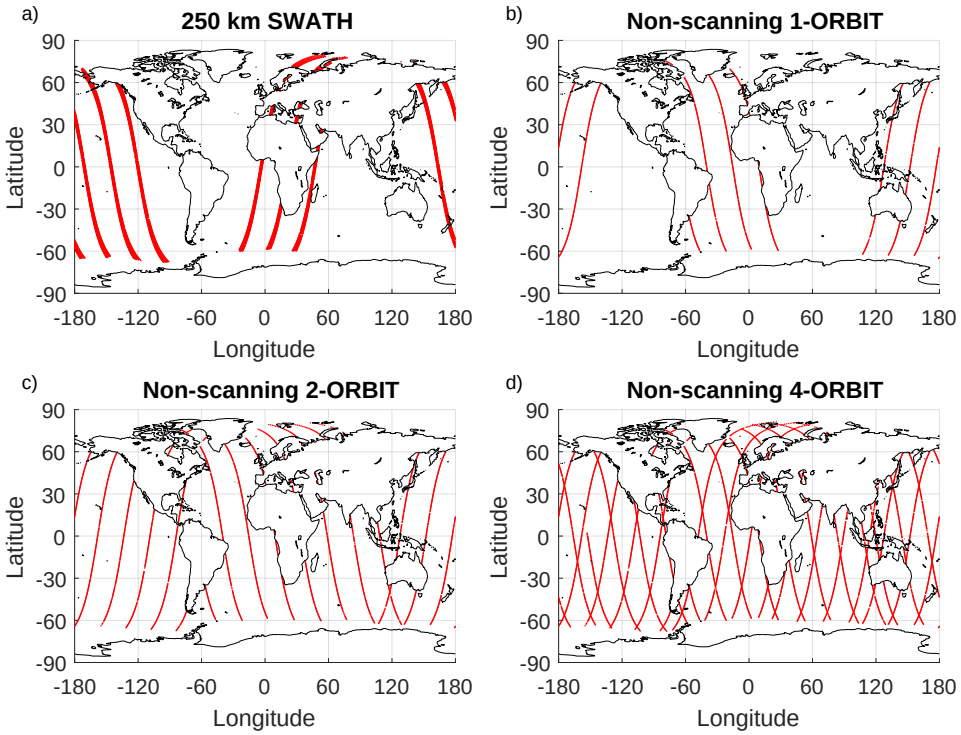


Figure 2. Comparison of orbits selected for experiments, showing observations for a six-hour window centered on 0000 UTC 01 July. a) Swath with 250 km scan; b) Non-scanning single orbit platform; c) Non-scanning with two orbital platforms; d) Non-scanning with four orbital platforms.

also more sporadically distributed contaminated observations in areas of generalized deep convection such as the west Pacific. A small fraction of SMSP observations are also excluded along coastlines due to the use of the 50 km footprint in the RAINCONT case.

Figure 3 compares the impact of SMSP observations on the RTMSE surface pressure analysis error for the month of September for the NOCONT and RAINCONT cases. Note that land regions and areas of sea ice are masked due to noisy orographic effects introduced by regridding of the G5NR and lack of SMSP observations. The global effect of considering rain contamination is minor, which is expected due to the slight reduction in the count of ingested SMSP observations. A slight weakening of beneficial SMSP impacts are found in the extratropics for the RAINCONT case, indicated by the light yellow areas in Figure 3c, on the order of 1-2% difference versus Control RTMSE. Some limited areas of greater difference in the Arctic Ocean are due to the removal of observations along the coastlines of Greenland, Svalbard, and Franz Josef Land.

The subtropics feature some regions where the SMSP impact is more beneficial in the RAINCONT case, indicated by the light blue areas in Figure 3c. The subtropics are regions where subsidence dominates, with less convection and heavy precipitation, so relatively few SMSP observations would be expected to experience rain contamination in these areas. These regions of improved impacts are likely the result of the use of the 50 km footprint, which is close to the resolution used by the DAS, resulting in less representativeness error in the simulated observations for the RAINCONT case compared to the point-interpolated observations in the NOCONT case. Any small-scale anomalies in

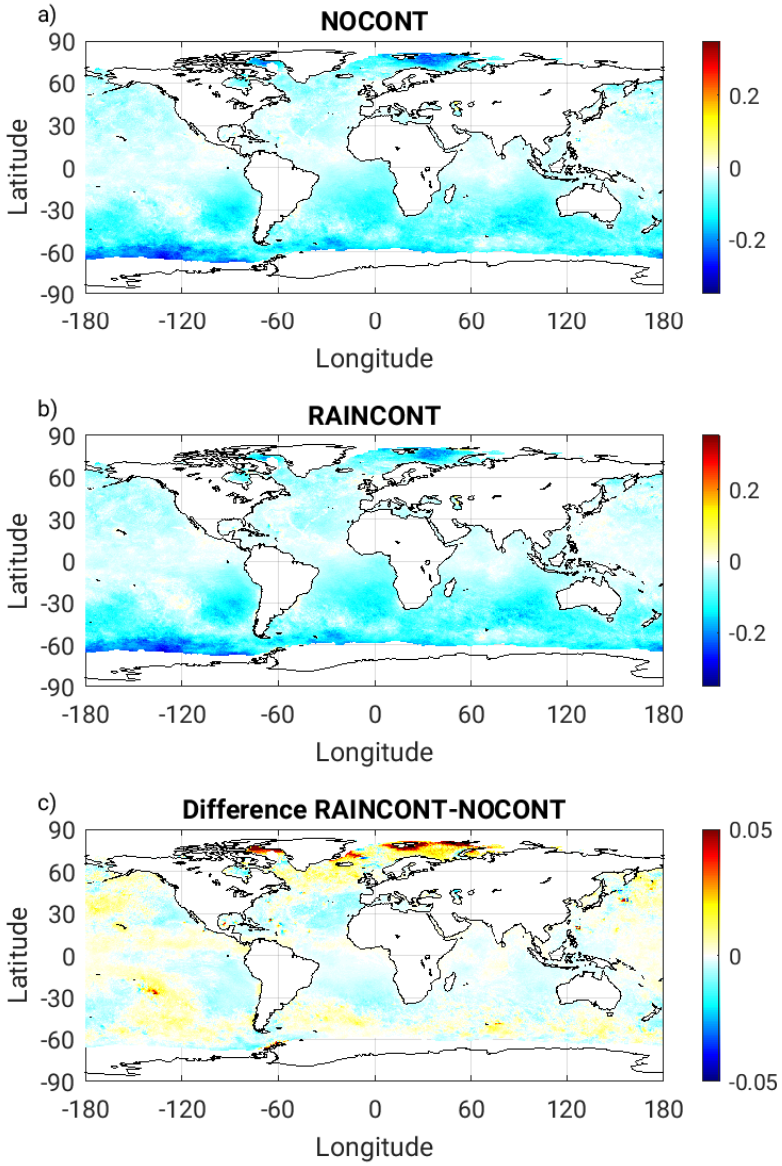


Figure 3. Comparison of RTMSE surface pressure analysis error impacts for the month of September for the case where rain contamination is considered versus the case where rain contamination is ignored. a) Fractional difference in RTMSE for the NOCONT case. b) as in a) but for the case in which rain contamination is included. c) Difference in fractional impact between the RAINCONT and NOCONT (note different color scale).

surface pressure can have an effect as of noise or observation error from the perspective of the DAS.

3.1.2 Tropical Cyclones

While the global effects of rain contamination on SMSP observations are small, larger effects can be expected in the vicinity of specific phenomena such as tropical cyclones and baroclinic lows. Several overpasses of tropical cyclones by the simulated SMSP instrument are considered to evaluate how rain contamination affects the SMSP impact.

Figure 4 illustrates four case studies where the SMSP swath overpasses a tropical cyclone, with the NOCONT case in the left column and the RAINCONT case in the right column. The location of the SMSP observations are indicated by black dots, with SMSP observations removed by quality control as magenta stars. Black contours show the background surface pressure error field, with solid contours indicating that the background cyclone pressure is too high compared to the NR. Dipoles of solid and dashed line anomalies indicate that the background tropical cyclone is displaced compared to the true location. Color shading indicates the analysis increment due to the ingestion of SMSP data.

The first case study example occurs on 03 September at 0600 UTC, where the background field has a tropical cyclone that is too weak compared to the NR and displaced slightly to the southwest, having a significant positive pressure error. The SMSP swath passes directly over the tropical cyclone. In the NOCONT case, one SMSP observation is rejected near the center of the tropical cyclone, where the observation innovation (O-B) of the observation exceeds the quality control criteria even though the observation is accurate. The analysis increment in the NOCONT case is generally aligned with the background error field, and causes the pressure to be reduced and the storm to be strengthened but the cyclone location is not appreciably shifted. In the RAINCONT case, a substantial number of SMSP observations are contaminated by rain in the vicinity of the tropical cyclone, however the overall structure of the analysis increment due to the SMSP is quite similar to the NOCONT case, just with weaker magnitude.

The second overpass example occurs on 08 September 1800 UTC, with a direct pass over a tropical cyclone that is displaced to the northwest of the true location, indicated by the positive-negative dipole in the background surface pressure error field. In the NOCONT case, two SMSP observations are omitted by quality control due to large O-B near the center of the tropical cyclone. While the increment acts to correct the background error on the northwest side of the cyclone, there is not a dipole structure to the increment and the cyclone shifts only very slightly to the southeast. The relatively long horizontal length scale of the increments compared to the error structure, along with the exclusion of some SMSP observations near the storm center result in this lopsided increment. In the RAINCONT case, more SMSP observations near the true cyclone location are excluded, and the positive increment on the northwest side is actually stronger than in the NOCONT case as the influence of these observations is removed.

In a third example, the SMSP sideswipes a tropical cyclone on 18 September 0600 UTC. Here, the background cyclone is weaker than the NR cyclone and shifted slightly to the south, with an area of positive background error centered over the tropical cyclone. In the NOCONT case, the increment due to the SMSP observations is significant in magnitude and nearly colocated with the background error field despite the fact that the overpass only partially crosses over the cyclone, and misses the storm center entirely. The cyclone is strengthened but not shifted in location. However in the RAINCONT case, the majority of observations in the vicinity of the cyclone are contaminated by rain, and the increment reflects an area of too-low background surface pressure well to the north of the cyclone. The net effect of the SMSP observations in the RAINCONT case acts to slightly weaken the tropical cyclone

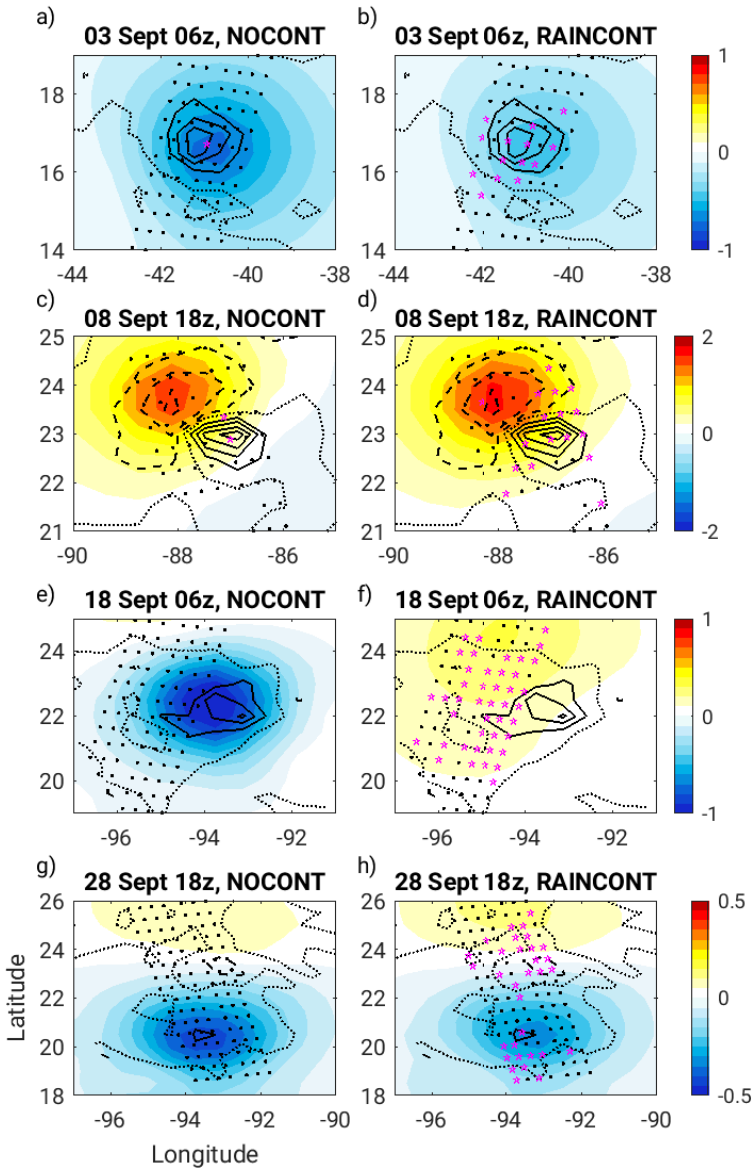


Figure 4. Four tropical cyclone overpass case studies, showing the effects of rain contamination of observations. Solid (dashed) black contours indicate the positive (negative) surface pressure error of the Control analysis state at 2 hPa contour intervals. Colored shading indicates the surface pressure (hPa) analysis increment caused solely by the inclusion of SMSP data. Black dots indicate SMSP observations ingested by the DAS. Magenta stars indicate SMSP observations removed by quality control.

In the fourth and final example, the background tropical cyclone is slightly weak and slightly displaced to the south of the NR cyclone. In the NOCONT case, the SMSP directly overpasses the cyclone and none of the observations are excluded by quality control due to the smaller magnitude of the O-B. The SMSP increments are centered over the background error and act to strengthen the tropical cyclone but do not shift the center of the cyclone. In the RAINCONT case, contaminated observations occur away from the center of the cyclone, resulting in modestly weaker increments from the SMSP observations compared to the NOCONT case.

These four examples were selected to illustrate the range of SMSP impact characteristics for tropical cyclones. The resulting impacts are very mixed, depending on specifics of the existing inaccuracies of the tropical cycle representation in the background, the coverage of the tropical cyclone by the SMSP overpass, and the distribution of rain. Due to the length scales used by the DAS for analysis increments, even dense coverage of a tropical cyclone by SMSP observations would not yield a highly structured increment or correction to the tropical cyclone surface pressure field. This type of mixed result, particularly in the presence of strong convection, can be expected to occur for other types of strong, localized surface pressure anomalies, such as baroclinic lows. As DAS techniques improve, and model resolution increases, SMSP observations might be able to provide better corrections for tropical cyclones and other smaller-scale pressure phenomena.

3.2 Observation Errors

As the SMSP is a new technology, the instrument error characteristics are not well understood. It is hoped that the SMSP would have on the order of 1-2 hPa standard deviation accuracy for retrieved surface pressure, corresponding to 0.1-0.2% of the measurement. From the perspective of the DAS, observation error consists of more than just the instrument error, also including representativeness error and observation operator error. The DAS uses an estimate of the total observation error as an assigned weighting function that determines the relative contribution of a particular observation in comparison to observations from other instruments and to the background model field. Smaller assigned observation error estimates tend to result in larger observation impacts, but estimations that do not correctly align with the true observation error will tend to weaken impacts, or even result in degradation of the analysis state.

In order to understand the accuracy requirements for an SMSP instrument, a series of twenty standalone cases were performed in which simulated random uncorrelated observation error is added to the simulated SMSP observations. Four different magnitudes of simulated errors were added: no error, 1 hPa, 2 hPa, and 4 hPa standard deviation random error. These four SMSP datasets are referred to as NOERR, 1-ERR, 2-ERR, and 4-ERR respectively. A small amount of intrinsic error is present in the NO-ERR dataset, largely due to representativeness error between the 7-km NR and the approximately 50 km DAS. However, the use of the 50 km footprint for the simulated SMSP observations causes this representativeness error to be small, although some error is introduced due to the use of temporal interpolation. Five different magnitudes of DAS-assumed error are tested for each level of added simulated SMSP error: 0.5 hPa, 1 hPa, 2 hPa, 4 hPa, and 6 hPa standard deviation SMSP error. The higher the error assumed by the DAS, the weaker the weighting of the observational data when generating an analysis. A one-month period for July is run in standalone mode for each of the twenty cases.

Figure 5 shows the normalized area averaged global marine surface pressure RTMSE compared to Control for each case as a function of the GSI assigned SMSP error magnitude. The solid line with stars illustrates the NOERR cases, with decreasing SMSP impacts as the GSI assigned error increases, i.e. as the SMSP observations are deweighted by the DAS. The curve for the NOERR case is nearly linear, and can be extrapolated

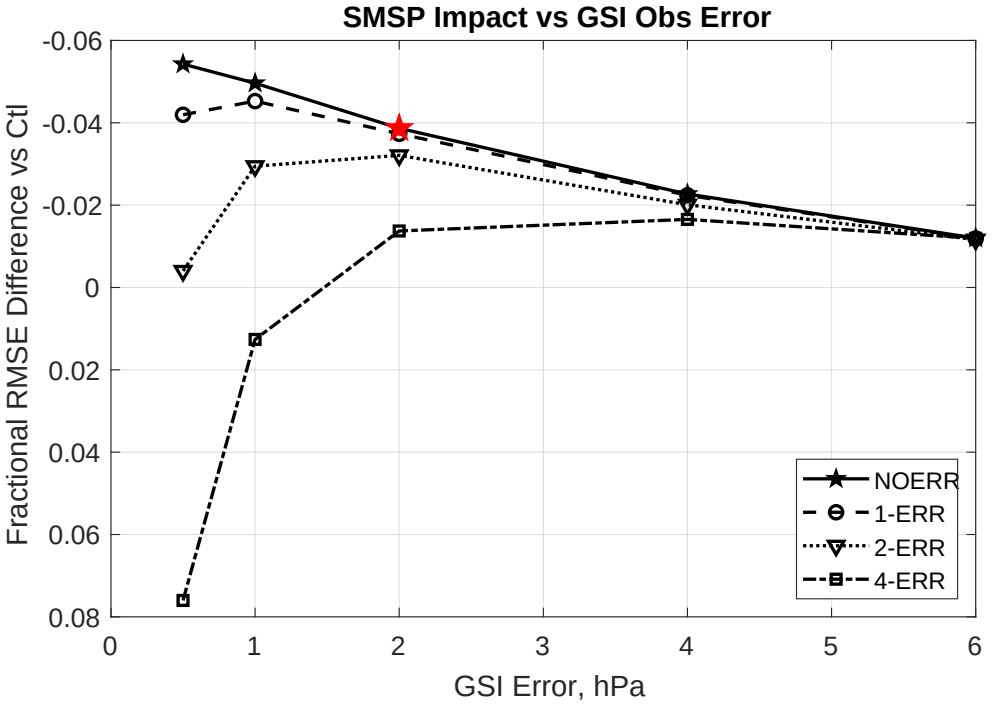


Figure 5. Comparison of the role of assigned GSI error weighting with the role of actual simulated observation error on the impact of SMSP observations on the marine surface pressure analysis. Y-axis, fractional change to areal averaged global marine surface pressure RTMSE compared to the OSSE Control and normalized by the Control. Abscissa, assigned observation error standard deviation for the SMSP assumed by the GSI, hPa. Solid line with stars, NOERR case. Dashed line with circles, 1-ERR case. Dotted line with triangles, 2-ERR case. Dash-dot line with squares, 4-ERR case. Red star indicates the configuration used in the orbit comparison experiments.

to the intersection with the y-axis, estimating that the total information content of the SMSP observations would ideally yield a 6% reduction (improvement) in the global marine surface pressure analysis error. The linear form of the NOERR curve indicates that the representativeness error of the simulated SMSP observations is small - likely below 0.5 hPa. The red star indicates the scenario that was used for the orbital configuration and rain contamination experiments. If the NOERR case were extrapolated out to larger assigned GSI errors, it is expected that the curve would asymptote to zero but would not change signs.

The 1-ERR, 2-ERR, and 4-ERR curves in Figure 5 demonstrate the expected behavior in which the optimal use of the SMSP observations occurs when the assigned GSI error matches the actual SMSP observation error. The peak SMSP impact for 1-ERR occurs for GSI assigned error of 1 hPa magnitude, the peak for 2-ERR at GSI assigned error of 2 hPa magnitude, and the peak for 4-ERR occurs at GSI assigned error of 4 hPa. For GSI assigned error greater than the added simulated error magnitudes, the behavior is similar to that seen in the NOERR case, with a gradual lessening of SMSP impacts. However when the SMSP is overweighted, with larger magnitude of added simulated SMSP error compared to the assigned GSI error, there is a steep drop-off in SMSP impacts as the GSI assigned error is decreased below the actual SMSP observation error magnitude.

For the 4-ERR case, the SMSP observations begin to degrade the analysis for GSI weighting below 2 hPa.

3.3 Orbital Configurations

Four different orbital configurations for an SMSP are tested, as depicted in Figure 2. In the SWATH configuration, the orbit is based on ATMS, with a scan width of 250 km and observation spacing of approximately 50 km. Three combinations of a constellation of 'small-sat' type orbits with a non-scanning instrument are tested, with one, two or four orbiting platforms (1-ORBIT, 2-ORBIT, and 4-ORBIT cases). In all four cases, 50 km footprints are used for the simulated observations, and rain contamination is also included. A three-month period of full-cycling mode is used from July-September, with 5-day long forecasts initialized at 0000 UTC each day.

Simulated SMSP observation errors were not added to the SMSP observations in these experiments, although the GSI weighting assumed SMSP errors of 2.0 hPa standard deviation. The configuration used is designated by the red star in Figure 5. For GSI assigned SMSP error of 2 hPa, the difference in net impact between the NOERR case and the 2-ERR case is relatively small, indicating that the orbital configuration experiments that do not include simulated observation error should be representative of the performance of a more realistic SMSP that includes errors on the order of 1-2 hPa standard deviation. Doubling the SMSP error to 4 hPa would result in the analysis impacts being approximately halved, but the SMSP would still provide beneficial impacts. The difference between 1 hPa and 2 hPa SMSP simulated observation error is on the order of 20% change in SMSP analysis impact for a GSI-assigned weighting of 2 hPa.

The impacts from the orbital configuration tests should be considered as a reasonable maximum potential impact that would be somewhat decreased depending on the magnitude and characteristics of the actual observation error. Due to the uncertainty in the performance characteristics of the SMSP instrument, particularly in terms of potential error correlations, this approach in conjunction with the error sensitivity studies in Section 3.2 was chosen in order to evaluate the full range of possible observation impacts.

3.3.1 Analysis Impacts

The impact of the SMSP observations for each orbital configuration can be calculated by comparing each case against the OSSE Control, using the NR for verification when calculating analysis and forecast errors. Figure 6 shows the three-month difference in RTMSE for the analysis surface pressure field for each case compared to Control, normalized by the Control analysis error. Negative values indicate a reduction in the analysis error when SMSP observations are included.

For the non-scanning SMSP configurations, increasing the number of orbital platforms results in greater beneficial impact of the SMSP observations. The most beneficial impacts are seen for the 4-ORBIT case compared to the other three orbital configurations, as illustrated in Figure 7b-d for impact comparisons of each non-scanning case to the SWATH case. The SWATH case has roughly similar magnitude impact as the 2-ORBIT case, with regional variations - greater beneficial impacts are noted near the Arctic Ocean in the SWATH case, but weaker beneficial impacts are seen over much of the Southern Ocean.

The spatial pattern of the SMSP impacts on the analysis surface pressure error is affected by the orbital geometry, regional atmospheric dynamics and physics, and the availability of other observing types. The Control RTMSE analysis surface pressure error is shown in Figure 7a, with greatest error in the Southern Ocean and along the Antarctic sea ice edge, with local regions of increased error in the south Atlantic, near the ITCZ

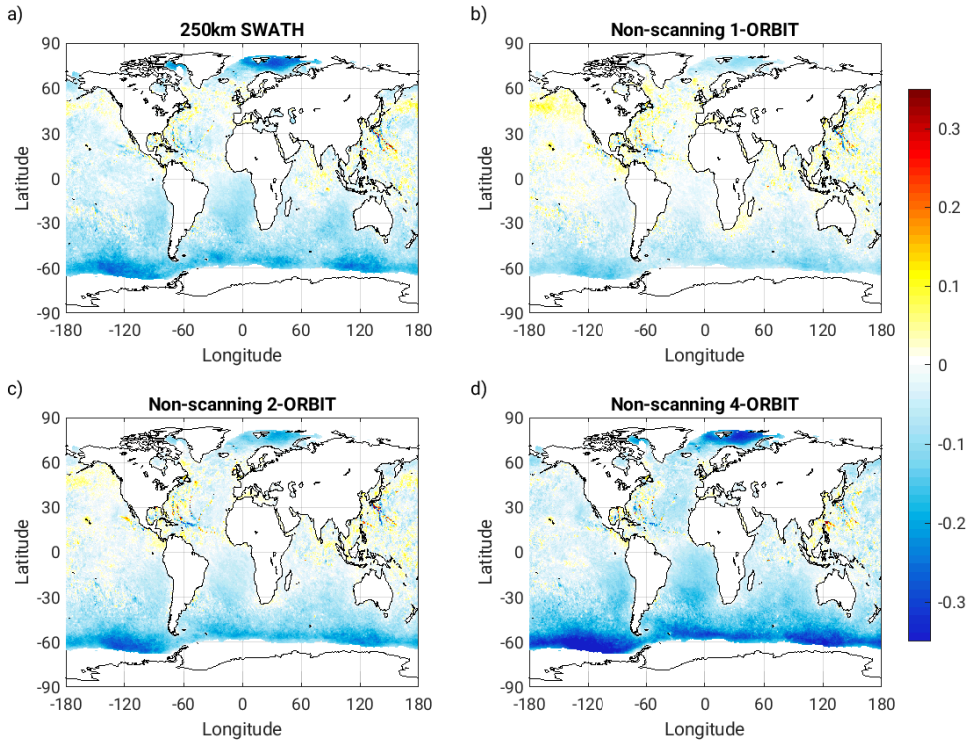


Figure 6. Fractional change to surface pressure analysis RTMSE compared to Control RTMSE (SMSP-Control)/Control, July-September. a) 250 km scan SWATH; b) non-scanning 1-ORBIT; c) non-scanning 2-ORBIT; d) non-scanning 4-ORBIT. Negative values indicate a reduction in error when SMSP observations are ingested.

in the Pacific, in the Arctic Ocean, and in regions of tropical cyclone activity such as the central Atlantic and east Pacific. Large beneficial impacts are seen in the Southern Ocean for all four orbital configurations, reflecting the large Control analysis errors available to correct, the lack of in-situ data in this region, and the relatively good coverage by the polar orbiting SMSP. Whereas in the tropics, where pressure gradients are weak, the Control analysis error is low and the SMSP orbital coverage is relatively sparse, resulting in only slight impacts of the SMSP observations.

Some areas of apparent degradation (yellow coloring in Figure 6) are noted that were not observed in the previously discussed standalone experiments (Figure 3a,b). This degradation is caused by feedbacks between the model physics that occur during the forward integration between cycle times in the full cycling experiments. Due to the dry mass constraint implemented in the data assimilation system, if surface pressures are adjusted in one location, small changes to surface pressure will be induced globally in order to retain the total atmosphere dry mass. In regions where the atmosphere is convectively or dynamically unstable, such as moist areas of the deep tropics, these small adjustments can cause convective processes to initiate, and a delayed response that results in a degraded background surface pressure state at the next cycle time can occur. This response does not occur in the standalone experiments because there is no forward integration of the model, and the background state is not changed as a result of the SMSP observations. This type of response has been noted for other data types (Privé et al., 2022).

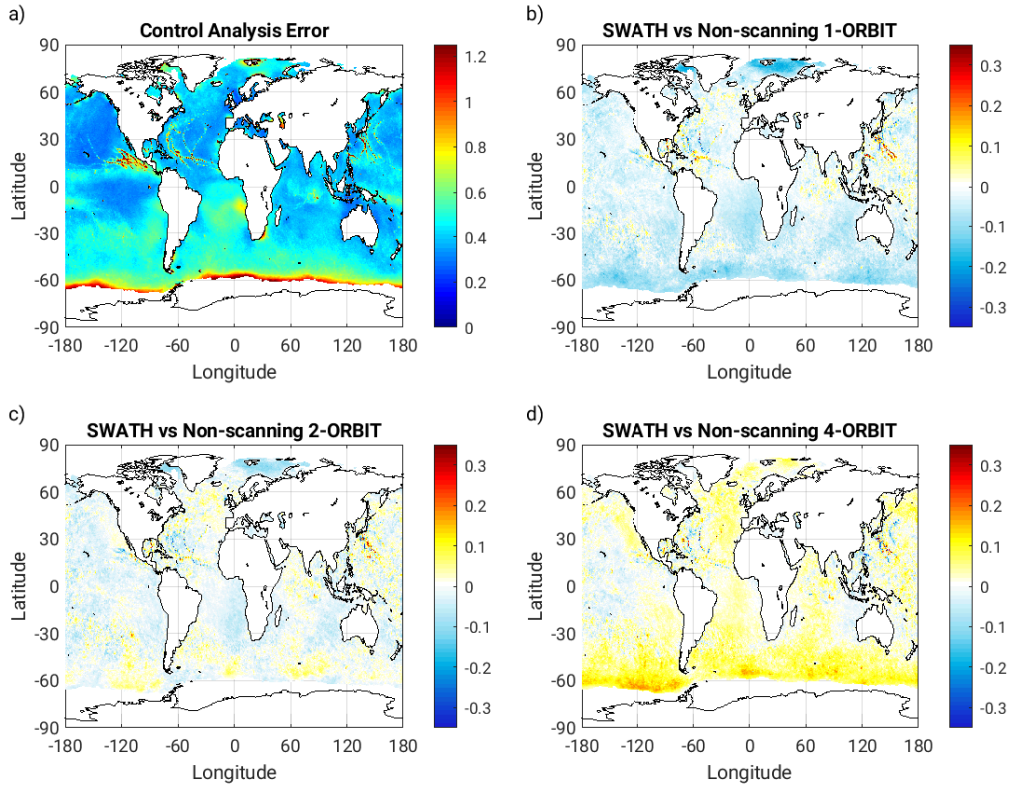


Figure 7. a) RTMSE Control surface pressure analysis error, hPa. b,c,d) Fractional change to surface pressure analysis RTMSE compared to Control RTMSE (SMSP-Control)/Control, July-September. b) Difference SWATH and non-scanning 1-ORBIT; c) Difference SWATH and non-scanning 2-ORBIT; d) Difference SWATH and non-scanning 4-ORBIT.

3.3.2 Forecast Impacts

Forecast impacts are calculated by comparing forecast errors for the SMSP experiments to the Control case, using once-daily 120 hour forecasts initialized at 0000 UTC over the three month experiment period. Figure 8 shows the SMSP impacts on RAMSE temperature forecast error as a fraction of Control forecast error for the four different orbital configurations separated into three regions.

As with the analysis impacts, the greatest SMSP forecast impacts are seen in the SHEX region for all orbital configurations. The 4-ORBIT case has the most beneficial impacts for the SHEX region, with improvements persisting for the first three days of the forecast period through the depth of the troposphere. The SWATH configuration has the second most beneficial impacts in the SHEX region, followed by the 2-ORBIT and 1-ORBIT cases, although beneficial impacts are found in all cases for the first two days in the lower troposphere. A striking feature in the extratropics most particularly for the 1-ORBIT case, and to a lesser extent for other cases, is the development of forecast degradation throughout the depth of the troposphere after approximately 72 hours and despite initial improvement.

In the NHEX region, weak beneficial impacts are found for all cases below 800 hPa in the first day of the forecast, with impacts that persist slightly longer into the forecast

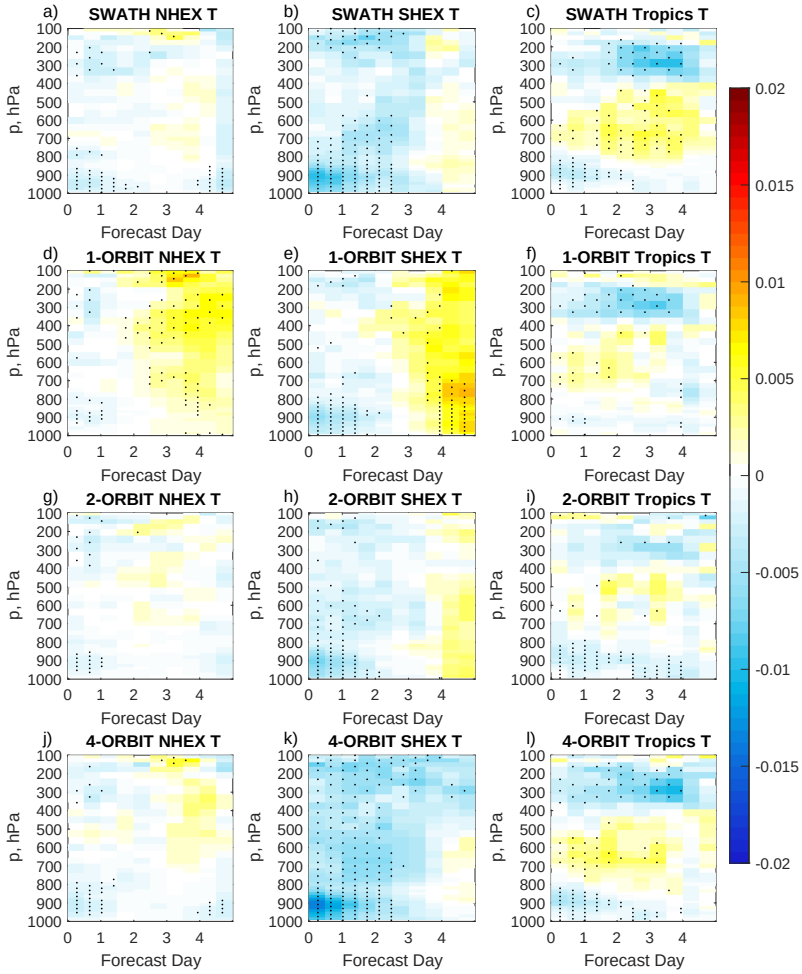


Figure 8. Fractional change to temperature forecast error compared to Control RAMSE when SMSP observations are included, normalized by Control RAMSE. Stippling indicates significance at the 90% level. a,b,c) SWATH; d,e,f) non-scanning 1-ORBIT; g,h,i) non-scanning 2-ORBIT; j,k,l) non-scanning 4-ORBIT. Left column, 20N-90N; center column, 20S-90S; right column, 20S-20N.

period for the SWATH case than for the non-scanning cases. In the Tropics, beneficial impacts are seen below 800 hPa and above 400 hPa, persisting for as long as 3-4 days in the SWATH and 4-ORBIT cases, but with mid-tropospheric degradation of the temperature forecast. This pattern of layers of improvement and degradation can be indicative of convective feedbacks in moist regions, where small changes to the analysis state set off deep convection that results in vertical redistribution of energy. Differences in the NR convective scheme and the forecast model convective scheme can result in layers of temperature changes that persist for several days into the forecast period.

Figure 9 shows SMSP impact on the specific humidity forecast, similar to Figure 8. Humidity impacts are somewhat weaker than those seen for temperatures, and ben-

eficial impacts of the SMSP instrument are primarily seen in the lower troposphere during the short term forecast period. The most beneficial humidity impacts are seen for the 4-ORBIT case in the SHEX region, where the greatest temperature forecast impacts were also found. Humidity is not directly observed by the SMSP instrument, and is only indirectly affected through mechanisms such as changes to the temperature fields, advection, and convective processes. It is thus not surprising that the humidity impacts are not as strong as the temperature impacts for SMSP data.

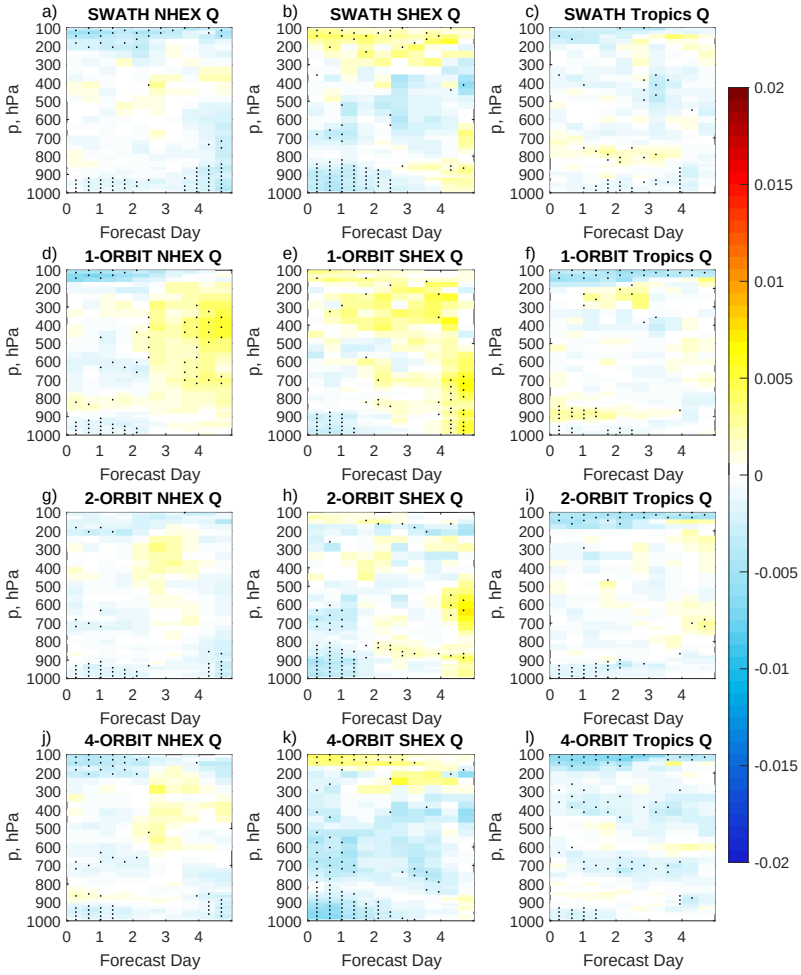


Figure 9. Fractional change to specific humidity forecast error compared to Control RAMSE when SMSP observations are included, normalized by Control RAMSE. Stippling indicates significance at the 90% level. a,b,c) SWATH; d,e,f) non-scanning 1-ORBIT; g,h,i) non-scanning 2-ORBIT; j,k,l) non-scanning 4-ORBIT. Left column, 20N-90N; center column, 20S-90S; right column, 20S-20N.

The SMSP impacts on zonal wind forecast skill are shown in Figure 10. The wind impacts are similar to those found for temperature in the southern hemisphere extratropics, with beneficial impacts extending to 24-48 hours, although the wind impacts do

not show a maximum in impact magnitude near 900 hPa that is seen for temperature. In the Tropics and northern hemisphere extratropics, wind forecast impacts are minimal, which is not unexpected due to the weak analysis impacts in those regions.

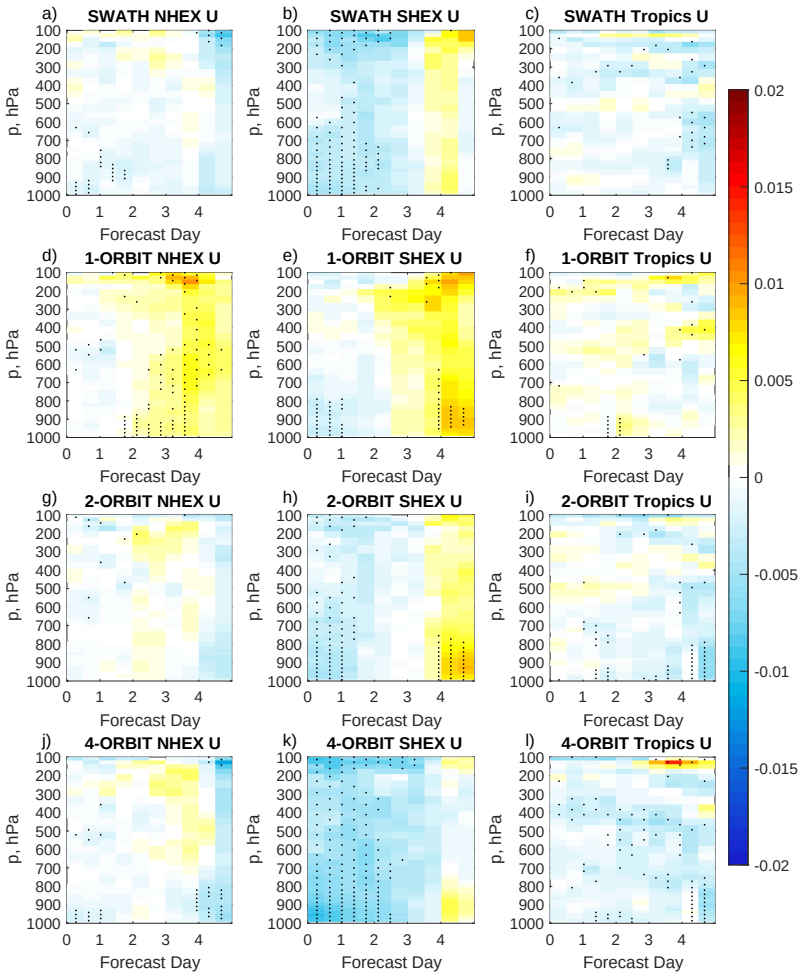


Figure 10. Fractional change to zonal wind forecast error compared to Control RAMSE when SMSP observations are included, normalized by Control RAMSE. Stippling indicates significance at the 90% level. a,b,c) SWATH; d,e,f) non-scanning 1-ORBIT; g,h,i) non-scanning 2-ORBIT; j,k,l) non-scanning 4-ORBIT. Left column, 20N-90N; center column, 20S-90S; right column, 20S-20N.

3.3.3 FSOI

Relative observation impacts of different data types on the 24-hour forecast skill are calculated using the FSOI tool, with total global wet energy error used as the norm. Figure 11 compares the FSOI for the four experiments, with the top bar for the SMSP instrument. Observations in three different regions are compared, using three months of forecasts at the 0000 UTC cycle time for the calculations.

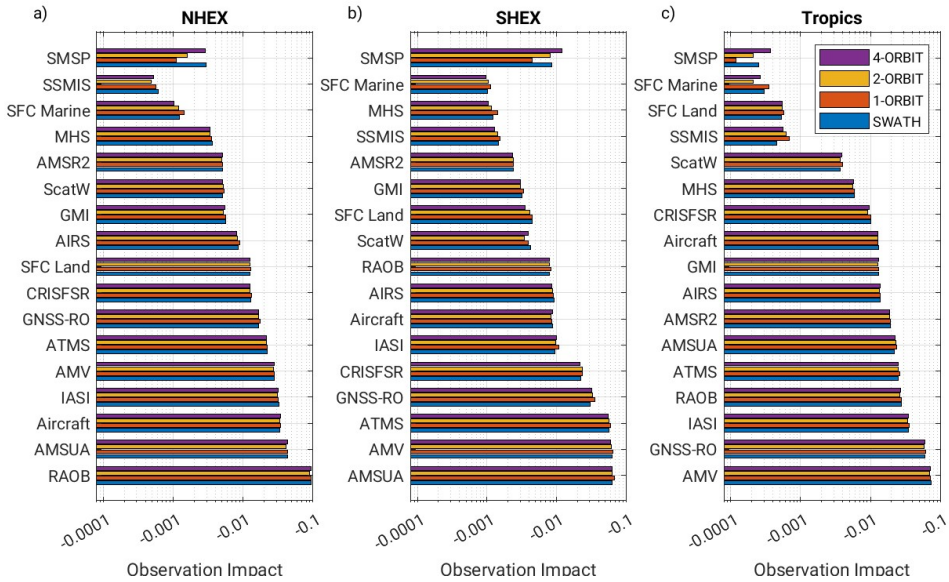


Figure 11. FSOI estimates of observation impact on the 24-hour forecast error norm for total wet energy, units J/kg. Note that the figures are semi-log. Left column, 20N-90N; center column, 20S-90S; right column, 20S-20N.

In the NHEX region, SMSP impacts are small but roughly on par with or slightly greater than the combined buoys, ships, and moored platform (SFC Marine) data. The 4-ORBIT case and the SWATH case have the largest impacts in the NHEX region, with more than twice the impact of ships and buoys in this area. The 1-ORBIT and 2-ORBIT cases have net impact similar to that of ships and buoys. Many of the conventional marine surface observation types in the NHEX region are moored platforms clustered along the coast, with relatively few observations in open ocean. In the Tropics, SMSP observations have minimal impact, similar to the conventional surface marine data. This aligns with the analysis and forecast impact results that show mixed to neutral SMSP impacts in the Tropics.

The largest SMSP impacts are seen in the SHEX region, which is expected based on the analysis and forecast impacts previously shown. The greatest SMSP impact in this region is found for the 4-ORBIT case, followed by the SWATH and 2-ORBIT cases. In this area, the SMSP impacts are much larger than the other surface marine types, and are on par with rawinsondes (RAOB), aircraft, and some radiance types such as AIRS and IASI. For the non-scanning constellation cases, the FSOI impact is not a linear function of the number of orbits. In the SHEX region, the 2-ORBIT case has slightly less than twice the impact as the 1-ORBIT case for SMSP, and the 4-ORBIT case has 40% greater impact than the 2-ORBIT case. This can be a sign of a certain degree of redundancy between the SMSP observations as additional non-scanning orbits are used.

FSOI impacts are granular, with a particular impact assigned to each observation, and the net impacts shown in Figure 11 are summations of many individual observation impacts. A mean per-observation impact can also be illuminating, and is shown in Figure 12. Per-observation impacts tend to favor instruments with relatively few observations, and accordingly the SMSP observations have quite high per-observation impact in the NHEX and SHEX regions, ranking near the top particularly for the non-scanning orbits.

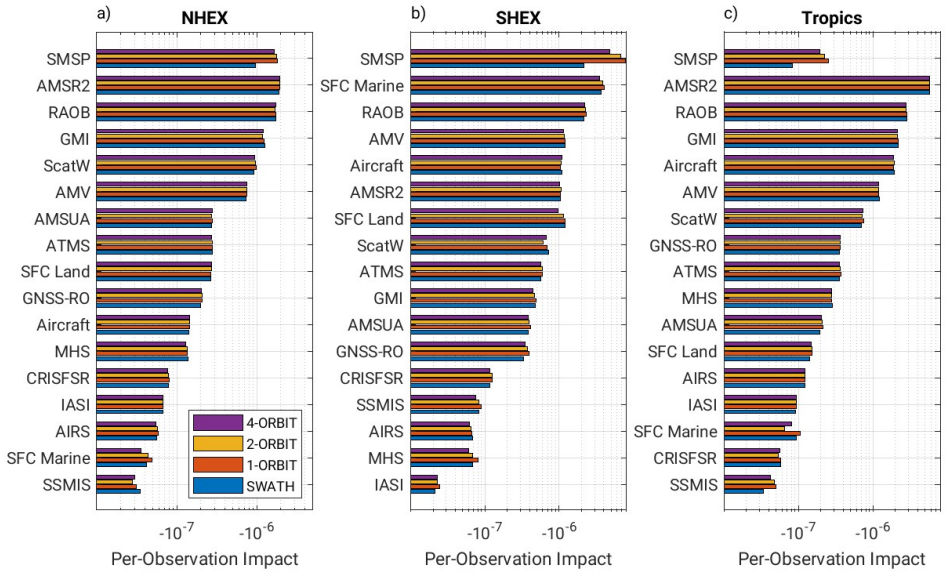


Figure 12. FSOI estimates of per-observation impact on the 24-hour forecast error norm for total wet energy. Left column, 20N-90N; center column, 20S-90S; right column, 20S-20N.

In the NHEX region, the largest per-observation impacts include several conventional types such as rawinsondes, AMVs, and scatterometer winds, along with two of the allsky radiance types - AMSR2 and GMI. The non-scanning SMSP per-observation impacts are competitive with rawinsondes and AMSR2, while the SWATH SMSP per-observation impacts are weaker, with impacts on par with AMVs. The SWATH SMSP observations have a certain degree of redundancy with each other due to the proximity of observations within the scan, accounting for the weakened per-observation impacts compared to non-scanning. Interestingly, ships, buoys, and other surface marine types have relatively small per-observation impact in the NHEX region, which may be due to the strong clustering of these data types along coastal areas, with relatively few observations in open ocean.

In the SHEX region, the non-scanning SMSP observations have the greatest per-observation impact of any type. Other surface marine observations have the second greatest per-observation impact, in contrast to the NHEX region. The relative importance of marine surface observations in the SHEX region may be due to the lack of coastal moored marine surface stations in this area, with ships and drifting buoys dominating the marine surface types. The SMSP SWATH per-observation impacts are similar in magnitude to that of rawinsondes in this region.

In the Tropics, the top ranked per-observation impacts are similar to those found in the NHEX region, however the SMSP per-obsevation impacts are much weaker than in NHEX. Other surface marine observations also have weak impacts in the tropics, and the SMSP observations are found to have roughly twice the magnitude of per-observation impact compared to ships and buoys. This may be due to the spatial distribution of SMSP being primarily over open ocean, while many of the ship routes and moored marine surface stations in the Tropics are near islands or close to continents.

An example of the spatial distribution of FSOI impacts for the 0000 UTC cycle is shown in Figure 13 by binning SMSP impacts according to observation location using 2° latitude/longitude areal bins. These impacts have a somewhat different distribution than that seen in Figure 6 for the analysis impacts. Some regions that show beneficial

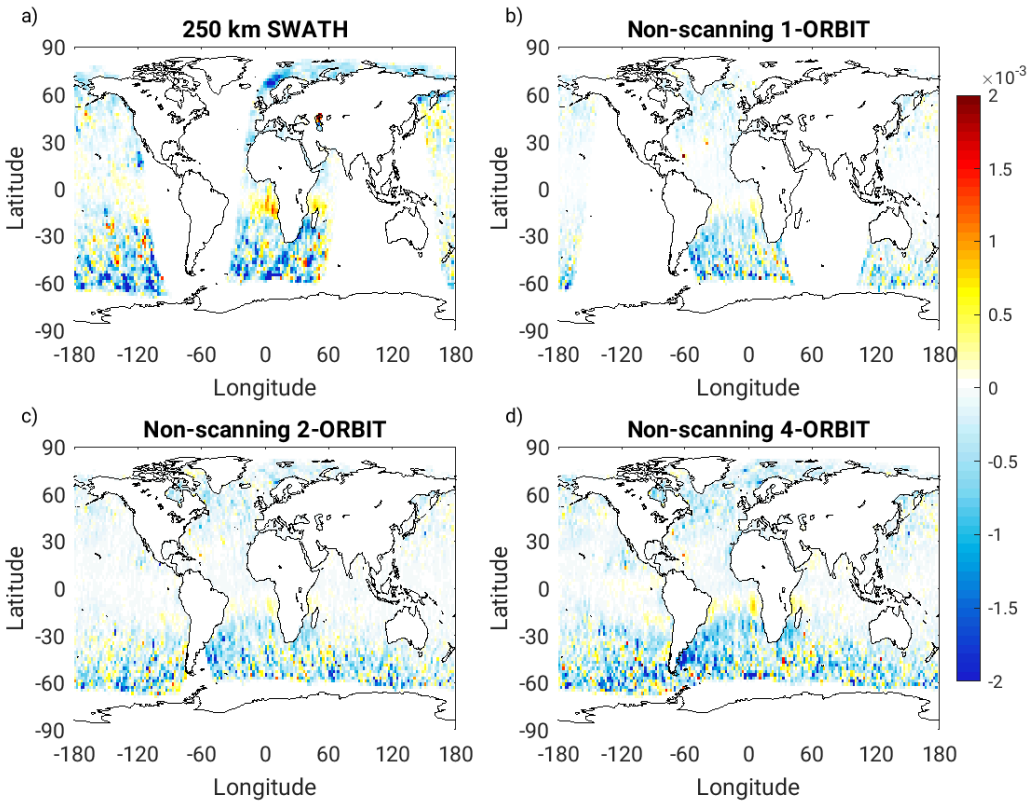


Figure 13. Three month accumulated FSOI impacts for the SMSP instrument for the 0000 UTC forecast cycle, units J/kg. Negative values indicate a beneficial impact of the SMSP observation on the 24-hour forecast total wet energy error norm. a) 250 km scan SWATH; b) non-scanning 1-ORBIT; c) non-scanning 2-ORBIT; d) non-scanning 4-ORBIT.

analysis impacts, such as the equatorial Atlantic Ocean off the coast of Africa, show degradation of the 24-hour forecast error norm. The region of the Southern Ocean just east of the southern tip of South America has relatively weak beneficial analysis impacts, but shows a stronger FSOI beneficial maximum, particularly for the 4-ORBIT case. The strong maximum in analysis impacts along the sea ice edge of Antarctica is not seen in the FSOI impacts. This implies that some of the background errors corrected by the SMSP observations may revert quickly due to fast model processes, while in other areas the SMSP observations act to correct slower growing errors such as in regions of strong baroclinicity.

The analysis and forecast impacts have shown mixed results, particularly in the tropics and Northern Hemisphere extratropics. This is due in part to inhomogeneities in the quality of the background field and the availability of observations, as well as limitations in the ability of the DAS to fully make use of the SMSP data. One metric that can help to quantify the usefulness of observations is the fraction of observations having a beneficial impact. Previous work has found that most observing types have a fraction of beneficial observations in the range of 50-55% (Gelaro et al. (2010), Lorenc and Marriott (2014), Hotta et al. (2017), Necker et al. (2018), Privé, Errico, Todling, and Akkraoui (2021). FSOI can be used to directly calculate the fraction of beneficial observations for different data types. The fraction of beneficial SMSP observations globally is 57.2% for the 1-ORBIT case, 56.9% for the 2-ORBIT case, 56.2% for the 4-ORBIT case, and 54.8%

for the SWATH case. This compares favorably with the fraction of beneficial in situ marine surface pressure observations of approximately 50%. Regionally, for the 4-ORBIT case, the fraction of beneficial SMSP observations is 58.5% in the SHEX region, 57.2% in the NHEX region, but only 52.5% in the Tropics. It is expected that the fraction of beneficial observations would decrease somewhat with the addition of simulated SMSP observation errors.

4 Discussion and Summary

Prior published OSSE studies of SMSP impacts (Privé, McLinden, et al., 2023) showed mixed results, with regions of improvement and of degradation, in large part due to issues associated with the use of a dry mass constraint by the incremental analysis update in the DAS. In the previous OSSE framework, there was a difference in the total atmospheric dry mass between the NR and the forecast model resulting in a surface bias of approximately 0.2 hPa at sea level. In combination with the dry mass constraint, corrections to the surface pressure under the SMSP swath lead to corresponding degradations in surface pressure in poorly observed areas, as discussed in detail by Privé, McLinden, et al. (2023). As a result, the SMSP impacts were fairly weak, especially for the 250 km wide scan orbital configuration, with greatest beneficial impacts over the tropical Pacific and near the polar oceans, and areas of degradation in the southern Indian Ocean.

In the updated OSSE, the dry mass constraint is still implemented, but the total atmospheric dry mass was adjusted in the quasi-operational NWP system and there is now a minimal bias compared to the NR dry mass. The SMSP impacts from the NO-RAIN case can be compared with the results shown in Privé, McLinden, et al. (2023) to illustrate the differences in impact in the previous OSSE version compared to the updated OSSE. The overall SMSP impact is much greater in the updated version, and the regions of greatest impact shift from the tropics to the extratropics, especially the poorly observed Southern Ocean and the Arctic Ocean. The tropical Pacific has weaker SMSP impacts in the updated OSSE due to the lack of surface pressure bias for the observations to correct along with the weak surface pressure gradients seen near the equator and complications from convective feedbacks. The new results are expected to be more representative of potential real world SMSP impacts, particularly as the use of a dry mass constraint in the DAS is relatively uncommon. The results also agree with studies of real drifter buoy surface pressure impacts (Ingleby & Isaksen, 2018; Reynolds et al., 2023) that found the largest observation impacts over the extratropical oceans especially in regions with strong baroclinicity.

In the previous OSSE, SMSP impacts in standalone mode were only 3% weaker than in full cycling mode, while in the updated OSSE, SMSP impacts in standalone mode are 30% weaker. In the previous OSSE, the mass redistribution caused by the dry mass constraint acted to adjust surface pressures far from the SMSP orbit, having the effect of erasing retained information from previous analysis cycles. In the updated OSSE, this mass redistribution is much reduced, and the SMSP information can be retained in subsequent analysis cycles. The difference between the standalone and full cycling impacts indicates that at each cycle time, 70% of the SMSP impact is due to the observations from the current cycle, while 30% is retained from previous cycles. Assuming exponential decay of observation impact with six-hour cycles, this implies a global half-life of SMSP information in the cycling of approximately four hours.

Case studies of SMSP overpasses of tropical cyclones help to both illustrate localized effects of rain contamination as well as to show how the DAS uses the SMSP observations. The SMSP observations are best able to correct errors in the strength of the tropical cyclone, such as decreasing the analysis surface pressure to strengthen the surface low. Correcting a displaced tropical cyclone appears to be more challenging - in this case, the error field will consist of a dipole structure of adjacent regions of negative and

positive error. Due to the horizontal length scale of the analysis increments associated with the SMSP observations, small-scale error features can be hard to correct. For tropical cyclones and also baroclinic lows, where precipitation can preferentially contaminate the SMSP observations over one section of the error dipole, the net effect of the SMSP observations may be simply to strengthen or weaken a displaced low rather than relocating the low in the correct direction. This behavior is not specific to SMSP data, but is intrinsic to how the DAS functions.

The role of SMSP observation error has been explored over a range of instrument accuracy levels. This can provide guidance for instrument design in determining target accuracies and whether design tradeoffs that would increase or decrease the observation accuracy are worthwhile. These tests show that if simulated SMSP observation errors are added to the simulated SMSP data in the expected range of 1-2 hPa accuracy, the SMSP impact would only modestly decrease compared to the impacts calculated without considering observation errors. The results also show that if the instrument were to have worse than expected performance, with accuracy of only 4-6 hPa, the SMSP observations would still have beneficial impact on NWP.

One aspect of observation error that was not addressed in these experiments was the effect of correlated observation errors. The DAS currently assumes that most observing types have uncorrelated observation errors, although this is an area of active research and advancement. Correlated observation errors tend to be treated by the DAS as if the errors were a true observation signal, and are not filtered or removed as easily as uncorrelated observation errors. The method that is often used to handle data types that have correlated errors is to de-weight the observations by assigning larger estimated observation error. For example, an SMSP instrument with 1 hPa standard deviation error that is significantly spatially correlated might be assigned an error level of 2 hPa in the GSI. The results of these experiments show that such a de-weighting would tend to incur a moderate reduction in SMSP impacts. The correlated errors would be expected to degrade the SMSP impacts somewhat in addition to the reduction in impact due to deweighting, although the extent of this would depend upon the character and magnitude of the correlations. Previous OSSE experiments comparing observation impacts with uncorrelated versus partially correlated errors (Privé, Errico, & McCarty, 2021) found that analysis and forecast impacts were significantly weaker in the presence of correlated observation errors.

For current instrument design and measurement concept, DAR return signals and retrievals are assumed to be independent. Correlated instrument errors for real data will be addressed through instrument calibration including calibration and comparison with in situ measurements. Also, rigorous calibration processes will be applied to DAR measurements, the expectation is that biases should be small and significantly less than random errors. Some bias correction may be needed for direct assimilation methods as the DAR observations use V-band spectra that are commonly bias corrected, and because a moist radiometer is required to calculate the total surface air pressure.

Comparison of the different orbital configurations found that the most beneficial impacts overall occurred for the 4-ORBIT constellation, with the SWATH case having the second most beneficial impacts. The 1-ORBIT case has extratropical SMSP analysis impacts that are approximately 40% of the magnitude of the 4-ORBIT case, and the 2-ORBIT case has analysis impacts that are approximately 70% of the magnitude of the 4-ORBIT case. However, there is a larger difference in between the constellation cases for the forecast impacts, with impacts in the 4-ORBIT case persisting twice as long into the forecast in the SHEX region as the 2-ORBIT case, and with minimal impacts in the 1-ORBIT case. While the 2-ORBIT and SWATH case have similar analysis impacts, the SWATH case performs better in terms of the forecast impacts. These results indicate that the spatial distribution of SMSP observations plays an important role in determining how well the SMSP information is retained into the forward model integra-

tion. Although a 3-satellite non-scanning constellation was not tested, these results yield the expectation that such a constellation would outperform the SWATH case in terms of observation impact for the analyses and forecasts. Importantly, a scanning instrument is not necessary to achieve significant SMSP impacts, and a constellation of non-scanning satellites has competitive performance compared to a single scanning instrument.

The comparative results for the 2-ORBIT and SWATH cases illustrate that changes to the analysis impact do not necessarily infer changes to the forecast impact. This limits somewhat the use of the standalone analysis impact cases when attempting to estimate the effects of SMSP observation error on forecast impacts. The analysis and forecast impacts seen for the orbital configuration cases should be considered as an upper limit for a best case scenario. Correlations in the SMSP errors may differently affect the SWATH and non-scanning impacts, depending on the structure and characteristics of the correlations.

Some delayed forecast degradation is observed in the extratropics after initial forecast improvements, especially for the 1-ORBIT case. It is not clear what the exact mechanism is, however the delayed response along with the weakening of degradation with increased quantities of SMSP observations may point to an indirect cause. If making any adjustments to the surface pressure field results in non-local surface pressure adjustments due to the dry mass constraint, these adjustments could tend to produce forecast degradation due to dynamical or physical processes. When relatively few SMSP observations are available, the direct impacts of the SMSP are weaker and relatively brief, revealing this degradation after 2-3 days. When more SMSP observations are available, the beneficial direct SMSP impacts may mask or overwhelm any indirect effects entirely or at least for a longer period.

The FSOI tool allows observation impacts of the SMSP instrument to be put into context with the global observing network. While for the Tropics region, SMSP impacts are on par with the combined impact of conventional marine surface types, the SMSP outperforms conventional marine surface observations in the extratropics. The SMSP observations are especially impactful in the southern hemisphere extratropics, where they outperform not only the conventional surface marine data, but also a number of radiance instruments. These strong regional impacts are likely due to a combination of factors including the sparsity of in-situ observations, the large areal fraction of ocean, and also the seasonality. Winter seasons in the extratropics feature strong surface pressure gradients and baroclinic lows, where surface pressure observations may have particularly valuable input.

In these experiments, SMSP observations have been omitted over sea ice because the reflectivity of sea ice at the V-band frequencies used by the radar is not well understood. It is possible that some SMSP measurements may be available over sea ice. As the magnitude of analysis errors of surface pressure over the Arctic and Antarctic sea ice regions are large (1-2 hPa RMSE) compared to over open ocean (generally below 1 hPa RMSE), any SMSP observations over these areas may have especially large, beneficial impacts. More detailed studies are needed to determine the possible performance of the DAR instrument over ice surfaces.

These experiments have explored the potential value of SMSP observations in the context of the current global observing network. Ongoing OSSE studies are planned to evaluate the use of an orbit with 65° inclination to provide better coverage of the midlatitudes. Future work should include the development of an observation operator to fully simulate the DAR observations, and integration of such an operator into the DAS in preparation for the use of real SMSP data. OSSE experiments could be performed to examine the effects of SMSP observation correlations. SMSP performance could also be explored using a baseline global observing network that represents expected future changes to the spaceborne and in situ observational suite.

5 Open Research

The full GEOS-5 Nature Run (Global Modeling and Assimilation Office, NASA, 2014) is available for download from a portal at `https://gmao.gsfc.nasa.gov/global_mesoscale/7km-G5NR/`

The codes used to generate simulated observations (R. Errico, 2023) are available on zenodo at `https://doi.org/10.5281/zenodo.11387384`

The GEOS/GSI version used for the experiment runs (NASA/GMAO, 2022) is available on zenodo at `https://doi.org/10.5281/zenodo.11387002`

Acknowledgments

The authors would like to thank Ron Errico (retired) for his longstanding efforts in developing the GMAO OSSE framework, and most recently in implementing the simulated all-sky observation types used in this manuscript. Support for this project was provided by the NASA Earth Science and Technology Office through the Instrument Incubator Program. Resources supporting this work were provided by the NASA High-End Computing (HEC) Program through the NASA Center for Climate Simulation (NCCS) at GSFC. The software for simulating GPSRO observations was provided by the Radio Occultation Processing Package (ROPP) of the Radio Occultation Meteorology (ROM) Satellite Applications Facility (SAF) of EUMETSAT, with the assistance of Sean Healy at ECMWF.

References

Centurion, L., Horányi, A., Cardinali, C., Charpentier, E., & Lumpkin, R. (2017). A global ocean observing system for measuring sea level atmospheric pressure: effects and impacts on numerical weather prediction. *Bull. of the Amer. Met. Soc.*, *98*, 231-238. (doi:10.1175/BAMS-D-15-00080.1)

Culverwell, I., Lewis, H., Offiler, D., Marquardt, C., & Burrows, C. (2015). The radio occultation processing package, ROPP. *Atmos. Meas. Tech.*, *8*, 1887–1899. (https://doi.org/10.5194/amt-8-1887-2015)

Ding, S., Yang, P., Weng, F., Liu, Q., van Delst, P., Li, J., & Baum, B. (2011). Validation of the community radiative transfer model. *J. Quant. Spectrosc. Radiat. Transfer*, *112*, 1050–1064. (doi:10.1016/j.jqsrt.2010.11.009)

Errico, R. (2023). *GMAO OSSE for Weather Analysis Software Package: Version 3* [Software]. Retrieved from `https://doi.org/10.5281/zenodo.11387384` doi: 10.5281/zenodo.11387384

Errico, R., Privé, N., Carvalho, D., Sienkiewicz, M., Akkraoui, A. E., Guo, J., ... Moradi, I. (2017). *Description of the GMAO OSSE for Weather Analysis software package: Version 3* (Tech. Rep. No. 48). National Aeronautics and Space Administration. (NASA/TM-2017-104606)

Errico, R. M., Carvalho, D., Privé, N. C., & Sienkiewicz, M. (2020). Simulation of atmospheric motion vectors for an observing system simulation experiment. *J. Atmos. Ocean Tech.*, *37*, 489–505. (doi:10.1175/JTECH-D-19-0079.1.)

Gelaro, R., Langland, R., Pellerin, S., & Todling, R. (2010). The THORPEX observation impact intercomparison experiment. *Mon. Wea. Rev.*, *138*, 4009–4025.

Gelaro, R., Putman, W. M., Pawson, S., Draper, C., Molod, A., Norris, P. M., ... Wargan, K. (2014). *Evaluation of the 7-km GEOS-5 nature run* (NASA/TM–2014-104606, No. 36). NASA.

Global Modeling and Assimilation Office, NASA. (2014). *GEOS-5 Nature Run, Ganymed Release* [dataset]. Retrieved from `https://gmao.gsfc.nasa.gov/global_mesoscale/7km-G5NR/`

Han, Y., van Delst, P., Liu, Q., Weng, F., Yan, B., Treadon, R., & Derber, J. (2006).

JCSDA Community Radiative Transfer Model (CRTM) - version 1 (NOAA Tech. Report 122).

Healy, S. (2013). Surface pressure information retrieved from GPS radio occultation measurements. *Quart. J. Roy. Meteor. Soc.*, *139*, 2108–2118.

Holdaway, D., Errico, R., Gelaro, R., & Kim, J. (2014). Inclusion of linearized moist physics in NASA's Goddard Earth Observing System data assimilation tools. *Mon. Wea. Rev.*, *142*, 414–433.

Horányi, A., Cardinali, C., & Centurion, L. (2017). The global numerical weather prediction impact of mean sea level pressure observations from drifting buoys. *Quart. J. Roy. Meteor. Soc.*, *143*, 974–985. (doi:10.1002/qj.2981)

Hotta, D., Chen, T., Kalnay, E., Ota, Y., & Miyoshi, T. (2017). Proactive QC: a fully flow-dependent quality control scheme based on EFSO. *Mon. Wea. Rev.*, *145*, 3331–3354. (doi.org/10.1175/MWR-D-16-0290.1)

Ingleby, B. (2010). Factors affecting ship and buoy data quality: a data assimilation perspective. *J. Atmos. Ocean Tech.*, *27*, 1476–1489.

Ingleby, B., & Isaksen, L. (2018). Drifting buoy pressures: impact on NWP. *Atmos. Sci. Lett.*, *19*. (https://doi.org/10.1002/asl.822)

Lawrence, R., Lin, B., Harrah, S., Hu, Y., Hunt, P., & Lipp, C. (2011). Initial flight test results of differential absorption barometric radar for remote sensing of sea surface air pressure. *J. Quant. Spectrosc. Ra.*, *12*, 247–253.

Lin, B., & Hu, Y. (2005). Numerical simulations of radar surface air pressure measurements at O2 bands. *IEEE T. Geosci. Remote*, *2*, 324–328.

Lin, B., McLinden, M., Cai, X., Heymsfield, G., Hu, Y., Privé, N., ... Li, L. (2024). Sea surface barometry with an O2 differential absorption radar: retrieval algorithm development and simulation. *Frontiers in Remote Sensing*, *5*. (doi:10.3389/frsen.2024.1399839)

Lin, B., McLinden, M., Heymsfield, G., Hu, Y., Privé, N., Li, L., ... Carswell, J. (2023). Simulations of sea surface reflection for V-band O2 differential absorption radar barometry. *Frontiers in Remote Sensing*, *4*. (doi:10.3389/frsen.2023.1105627)

Lorenc, A., & Marriott, R. (2014). Forecast sensitivity to observations in the Met Office Global numerical weather prediction system. *Quart. J. Roy. Meteor. Soc.*, *140*, 209–224. (doi: https://doi.org/10.1002/qj.2122)

Millán, L., Lebsock, M., Livesey, N., Tanelli, S., & Stephens, G. (2014). Differential absorption radar techniques: surface pressure. *Atmospheric Measurement Techniques*, *7*, 3959–3970. (doi:10.5194/amt-7-3959-2014)

NASA/GMAO. (2022). *Gridpoint Statistical Interpolation and Goddard Earth Observing System* [Software]. Retrieved from `https://doi.org/10.5281/zenodo.11387002` doi: 10.5281/zenodo.11387002

Necker, T., Weissman, M., & Sommer, M. (2018). The importance of appropriate verification metrics for the assessment of observation impact in a convection-permitting modelling system. *Quart. J. Roy. Meteor. Soc.*, *144*, 1667-1680. (doi.org/10.1002/qj.3390)

Privé, N. C., Errico, R. M., & Akkraoui, A. E. (2022). Investigation of the potential saturation of information from global navigation satellite system radio occultation observations with an observing system simulation experiment. *Mon. Wea. Rev.*, *150*, 1293–1316. (doi:10.1175/mwr-d-20-0256.1)

Privé, N. C., Errico, R. M., & McCarty, W. (2021). The importance of simulated errors in observing system simulation experiments. *Tellus A*, *73*, 1–117. (doi:10.1080/16000870.2021.1886795)

Privé, N. C., Errico, R. M., Todling, R., & Akkraoui, A. E. (2021). Evaluation of adjoint-based observation impacts as a function of forecast length using an observing system simulation experiment. *Quart. J. Roy. Meteor. Soc.*, *147*, 121–138. (doi: 10.1002/qj.3909)

Privé, N. C., McGrath-Spangler, E. L., Carvalho, D., Karpowicz, B. M., & Moradi,

I. (2023). Robustness of observing system simulation experiments. *Tellus-A*, *75*. (doi:10.16993/tellusa.3254)

Privé, N. C., McLinden, M., Lin, B., Moradi, I., Sienkiewicz, M., Heymsfield, G. M., & McCarty, W. (2023). Impacts of marine surface pressure observations from a spaceborne differential absorption radar investigated with an observing system simulation experiment. *J. Atmos. Ocean Tech.*, *40*, 897–918. (doi:10.1175/JTECH-D-22-0088.1)

Radnóti, G., Bauer, P., McNally, A., & Horányi, A. (2012). *ECMWF study to quantify the interaction between terrestrial and space-based observing systems on numerical weather prediction skill* (Tech. Rep. No. ECMWF Technical Memorandum 679). ECMWF.

Reynolds, C., Stone, R., Doyle, J., Baker, N., Wilson, A., Ralph, F., ... Centurioni, L. (2023). Impacts of northeastern Pacific buoy surface pressure observations. *Mon. Wea. Rev.*, *151*, 211–226. (doi:0.1175/MWR-D-22-0124.1)